Model of cw argon ion lasers excited by low-energy electron beams

G. J. Fetzer, J. J. Rocca, and G. J. Collins
Colorado State University, Fort Collins, Colorado 80523

R. Jacobs
Spectra Physics Inc., 1250 W. Middlefield Avenue, Mountain View, California 94039

(Received 12 May 1986; accepted for publication 11 July 1986)

A model of cw argon ion lasers excited by low-energy (50–200 eV) direct current electron beams at current densities between 1 and 50 A/cm^2 has been developed. The electron energy distribution in the electron-beam-created plasma is calculated by numerically solving the Boltzmann equation for electrons. Optical gains, powers, and laser efficiences were computed for the 4765-, 4880-, 4965-, and 4658-Å Ar II transitions for a wide range of discharge conditions. Laser efficiencies comparable to those of a conventional Ar II laser ($\sim 3\times 10^{-4}$) are predicted for these laser transitions when electron beam excitation is used.

I. INTRODUCTION

We have analyzed the feasibility of developing a cw argon ion laser cited by a low-energy (50–200 eV) electron beam, in hopes of demonstrating possible improved efficiency over conventional devices. The study was motivated by the idea that a beam of electrons having an energy close to the peak of the excitation cross section of the upper laser levels might excite these levels more efficiently than conventional discharges.

In conventional cw argon ion lasers the active medium is the positive column region of a high current density discharge.[1] For practical purposes the electron energy distribution in this region of the plasma can be described as a Maxwell–Boltzmann distribution with a mean energy of 3–8 eV, depending on the operating conditions.[2] The upper laser levels for the blue-green transitions in the argon ion laser are between 33 and 35 eV above the ground state of the atom. The cross sections for direct excitation of these levels peak between 60 and 100 eV.[3] Consequently, the overlap between the electron energy distribution and the cross sections for single-step excitation is small and two-step excitation is the dominant excitation mechanism in the positive column devices. However, two-step excitation requires electrons having an energy of more than 20 eV. Thus, the overlap of the electron energy distribution and the two-step excitation cross section is still not very good. Another limiting factor is that in the narrow bore discharges many of the ions will diffuse to the walls before they may be excited via another collision. The positive column blue-green argon ion laser typically has an efficiency of around 5×10^{-4} while the quantum efficiency is approximately 7%.[1] The question arises: It is possible to increase the excitation efficiency of the cw argon ion laser using an electron beam with an energy close to the peak of the direct excitation cross sections?

The earliest published experimental results of the operation of an argon ion laser medium excited by a low-energy electron beam corresponds to the work of Hammer and Wen.[4] They measured the optical gain of the Ar II blue-green transitions in a modified RCA 6Y6 triode with an active length of 2 cm. In this device, the electron beam propagates in a direction perpendicular to the optical axis. This will be referred to as transverse excitation. Hammer and Wen placed their triode device in the optical cavity of a conventional argon ion laser as a gain modulator. At an electron beam current density of 1.66 A/cm^2, a beam energy of 110 eV, and a gas pressure of 0.1 Torr, an optical gain of 0.2%/cm on the 4765-Å transition was measured. Experiments at higher current densities were not conducted. More recently, Hara *et al.*[5] have observed cw laser oscillation on the 4880-Å transition in a device in which a 50–200-eV electron beam was directed along the optical axis, i.e., a longitudinally excited laser. They have obtained 30 mW output power at an efficiency of 3.0×10^{-5}. Differential pumping was used to allow for a low-pressure region for electron beam generation and a higher-pressure region for light amplification. An axial magnetic field was applied to the discharge to contain the electron beam. It is interesting to note that, in contrast to Hammer and Wen, Hara *et al.* have observed oscillation only on the 4880-Å transition and none of the other well-known lines in Ar II.

We have developed a computer model of a stationary argon plasma sustained by a transverse electron beam, to model a device similar to Hammer and Wen's. We have also extended this model to consider the device of Hara *et al.*

The transverse device modeled in this work is similar to that used by Hammer and Wen[6] to study the excitation cross sections of the upper laser levels of Ar II by low-energy beam electrons. We have selected, for our calculations, a plasma length of 15 cm: a dimension that is more practical for an argon ion laser oscillator than the 2-cm length used by Hammer and Wen for the collision cross-section study. We have chosen the same active cross-sectional area of 0.3×0.3 cm^2 as that of Hammer and Wen's device so that gains calculated by the model may be compared to the available experimental results. In this work we considered current densities between 1 and 35 A/cm^2 at beam energies of 50–170 eV and gas pressures between 0.05 and 0.2 Torr. For the purposes of our calculations, the transmissivity of the accelerating grid was chosen to be 64%.[7] The proposed transverse laser, schematically shown in Fig. 1, operates in the following manner; Electrons emitted by a thermionic cathode are accelerated by the positively biased grid into a drift region similar to that described by Tien.[8] The beam electrons ionize the gas and cre-

 0021-8979/86/202739-15$02.40

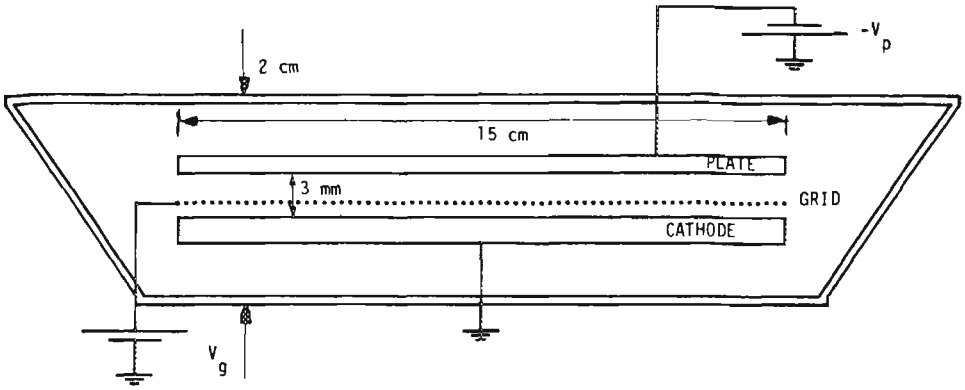

FIG. 1. Schematic diagram of transversely excited device modeled. Note that the drawing is not to scale.

ate a plasma in the drift region. Excitation of the laser upper levels is accomplished via single step and multistep electron-atom, electron-ion collisions. To more efficiently deposit the beam energy into the plasma, electrons which transverse the drift region are reflected by the negatively biased plate positioned parallel to the cathode. At the operating conditions considered the reaching distance of the beam electrons is such that they can traverse the drift region several times, ensuring a spatially uniform plasma.

The longitudinally excited electron beam laser modeled is described in Ref. 4. In this case the assumption of plasma uniformity is not well justified since the electron beam degrades in energy as it propagates in the active medium region of the device. However, the model predictions exhibit a good agreement with experimental results and explain the major trends observed in the actual laser. Predicted laser output powers are within a factor of 2 of the measured values.

In Sec. II we discuss the model of argon considered and the population density rate equations required to calculate laser gain, power, and efficiency for the 4880-, 4765-, 4965- and 4658-Å transitions of the argon ion. Section III contains results and predictions obtained through computer simulation of the devices discussed above. Our simulations indicate that an electron-beam-excited argon on laser does not offer improved efficiency over the positive column devices but will have a comparable efficiency. A summary of the conclusions obtained in this work is offered in Sec. IV. A collection of collision cross sections used in the model and curve fittings to these cross sections is offered in Appendix A.

II. THE MODEL

The goal of modeling these laser systems is to provide an estimate of the optical gain, laser output power, and efficiency for a variety of excitation conditions. In this section we discuss the components of the model. A model of the argon atom and ion is discussed in relation to calculation of the electron energy distribution and population densities of the ground-state ion and atomic metastable levels in the negative glow region of the discharge. The laser level populations, gain, power, and efficiency are then considered. Finally we describe a simple gas heating calculation incorporated in the model to estimate the gas temperature in the active region of the device.

A simplified model of Ar I and Ar II is used for the purposes of calculating the electron energy distribution. An energy diagram of this model is shown in Fig. 2. We have considered 13 excited states in the atom. The metastable states were also included to consider the effects of electron-metastable collisional ionization and Penning ionization. The metastable state considered here is actually a composite of the four lowest excited states of atomic argon. Resonant radiation from the $^3P_1$ and $^1P_1$ resonant levels is significantly trapped and these levels are added to the $^3P_0$ and $^3P_2$ metastable states to form a single composite state. The four states are closely spaced in energy (<0.3 eV) and the populations of each are strongly mixed by electron collisions. Consequently, treating these four levels as a single level for the purposes of calculating the contribution of two-step ionization is a reasonable assumption and simplifies calculations. Results further justify the approximation since two-step ionization in the electron-beam-created plasma was calculated to be less than 7% of the total ionization rate.

The system of equations used to calculate the ground-state ion and metastable densities, Ar^+ and Ar^*, is

$$\frac{d\,Ar^+}{dt} = 0 = R_I + R_I^* + c(Ar^*)^2 - \frac{Ar^+}{\tau_d^+} - \alpha N_i^2 Ar^+ , \tag{1}$$

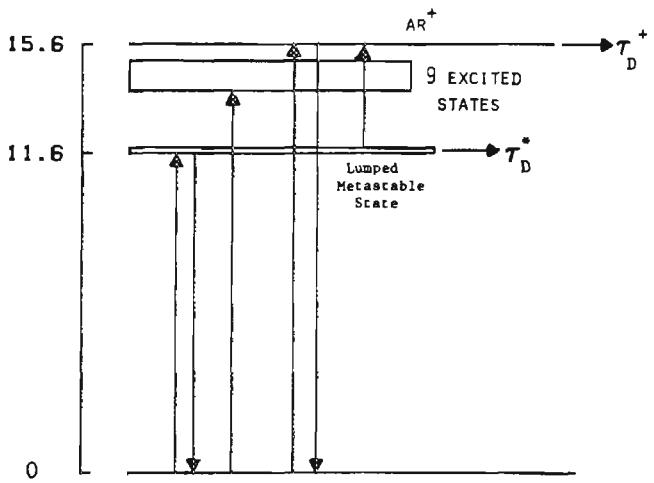

FIG. 2. Partial energy level diagram of Ar I and Ar II. These levels are used in the calculation of the electron energy distribution in the drift region.

$$\frac{d\,\mathrm{Ar}^*}{dt} = 0 = R^* - R_I^* - \mathrm{Ar}^*\left(\frac{1}{\tau_d^*} + R_{\mathrm{SE}}\right) - c(\mathrm{Ar}^*)^2. \quad (2)$$

Here R_I and R_I^* are the single-step and two-step electron impact ionization rates, respectively. R^* is the rate of formation of the metastable state by electron impact. The Penning ionization rate constant between two metastable atoms is represented by c. The diffusion time of ions and metastables are represented by τ_d^+ and τ_d^*, respectively. R_{SE} accounts for superelastic electron deexcitation of the combined metastable level. Under the discharge conditions considered here, three-body recombination is the dominant recombination reaction and radiative recombination is negligible. In Eq. (1) α is the three-body recombination coefficient and N_t is the thermal electron density.

The electron energy distribution in an electron-beam-created plasma is non-Maxwellian. We have numerically solved the Boltzmann equation for electrons to calculate the electron energy distribution. A recursive technique, based on an assumption of spatial plasma uniformity, suggested by Petersen[9] and later used by Warner[10] to model a helium hollow cathode discharge was used to calculate the electron energy distribution. The technique exploits the fact that an electron-beam-created plasma is practically free of an electric field. As such, beam electrons once introduced into the plasma are not subject to an accelerating force. By discretizing the energy space into a set of bins, the flow of electrons due to collisions with atoms, ions, and electrons is calculated in a top-down fashion. That is, starting with electrons at the beam energy due to collisions is tracked. Knowledge of the flow of electrons into and out of an energy bin allows the calculation of the density of electrons at that energy. Secondary electrons created in ionization collisions are included in the accounting procedure. The interested reader will find the details of the energy distribution calculation in Appendix B.

Figure 3 is a logarithmic plot of the electron energy distribution in the transverse device for a discharge voltage of $V_g = 170$ V, a current density of 1.66 A/cm^2, and a filling pressure of 0.1 Torr. Energy bin widths of 1 eV were used. The spike at the high-energy end of the distribution corresponds to the electrons introduced into the plasma at the beam energy that have not collided. At energies immediately below the beam energy we use a relatively low density of electrons. Electrons are produced in this region by elastic collisions and ionization of metastable atoms by beam electrons. The next high density region begins at $eV_g - E_1$ from the beam energy. The energy E_1 corresponds to the energy required to reach the first excited state of the neutral argon atom and is approximately 11 eV. Thus, a large number of beam electrons undergoes a collision resulting in an excited atom and electron with an energy $eV_g - E_1$. There is a similar increase in density at an energy of $eV_g - E_I$ corresponding to a beam electron undegoing an ionizing collision with a ground-state atom. The production of secondary electrons ionizing collision with a ground-state atom. The production of secondary electrons in ionizing collisions has two interesting effects on the electron energy distribution. The first of these is a consequence of the fact that in electron impact ionization the primary electron may impart a portion of its kinetic energy to the secondary electron produced in the collision. The continuous nature of the primary electron energy loss tends to smear the electron energy distribution. This can be seen in the middle section of the energy distribution which is quite smooth in comparison to the high-energy end. Secondly, the large increase of electrons at the low-energy end of the distribution is also due to the production of secondary electrons. The differential ionization cross section peaks at a secondary electron energy of zero. As a result, the density of

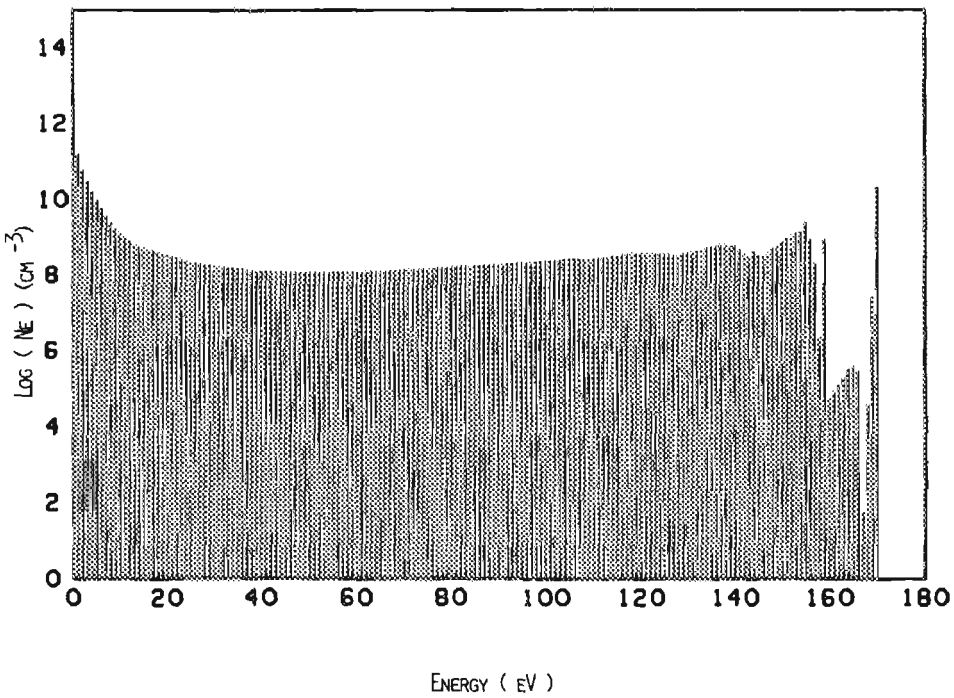

FIG. 3. Electron energy distribution of an electron-beam-created plasma $J = 1.11$ A/cm^2, $V_g = 170$ V, $P = 0.1$ Torr.

electrons at low energies becomes quite large due to the large number of low-energy secondaries produced in ionizing collisions. At very low eneriges the electron energy distribution is thermalized by elastic collisions. We have measured the average electron energy of this group of electrons in a helium plasma, created by a 1-keV electron beam for several pressures and current densities, finding values between 0.08 and 0.1 eV.[11] These results are in good agreement with measurements in other low-pressure discharges sustained by electron beams.[12,13]

Once the electron energy distribution and the ground-state ion density is known the populations of the $4p\ ^2P_{1/2,3/2}$, $4p^2D_{3/2,5/2}$, and $4s^2P_{3/2,1/2}$ levels of Ar II are calculated solving a set of population density rate equations. Knowledge of these densities allows the calculations of the optical gains of the 4765-, 4880-, 4965-, and 4658-Å laser transitions of Ar II.

Figure 4 is a partial energy level diagram of argon and illustrates the processes of excitation and deexcitation considered for calculation of the upper and lower laser level populations. The particular energy levels in Fig. 4 correspond to the levels of the 4880-Å laser transition. The energy levels of the remaining transitions are treated in a similar fashion. For the purpose of calculating the small signal gain the equation for the ith upper laser level population N_{ui} has the form

$$\frac{dN_{ui}}{dt} = 0 = R_{du} + R_{mu} - N_{ui} \sum_j (A_{ij} - N_t D_{ij}), \quad (3)$$

while the lower laser level populations N_p are calculated solving an equation of the form

$$\frac{dN_p}{dt} = 0 = R_{dp} + R_{mp} + \sum_{i=1}^{2} N_{ui}(A_{ip} + N_t D_{ip}) - N_p \sum_j (g_j A_{pj} + N_t D_{pj}), \quad (4)$$

where R_{du} and R_{dp} are the rates of direct excitation of the upper and lower laser levels by electron impact from the atomic ground state and R_{mu} and R_{mp} are the rate of excitation of the upper and lower level from the argon ion ground state. Contributions due to radiative cascade from higher energy states are included in these rates. A_{ip} is the spontaneous emission coefficient from the upper level i to the lower level p, as listed by Weise *et al.*[14] The factor g_j, as derived by Holstein,[15] corrects the lower level spontaneous emission coefficient, A_{pj}, accounting for trapping of the resonant radiation. Electron impact deexcitation rate constants are represented by D_{ij}. The pumping rates to upper levels are calculated as

$$R_{du} = \sum_{k=I_u}^{K} Ne(k)v(k)Q_u(k)\mathrm{Ar}, \quad (5)$$

$$R_{mu} = \sum_{k=I_{mu}}^{K} Ne(k)v(k)Q_{mu}(k)\mathrm{Ar}^+, \quad (6)$$

where I_u and I_{mu} are the energy bins corresponding to the upper laser level excitation threshold from the ground-state atom and the ground-state ion. $Ne(k)$, $v(k)$, and $Q(k)$ are the electron density, the velocity, and cross section at a discrete energy represented by the index k. K is the energy bin index corresponding to the energy of the injected electron beam.

Collisional deexcitation of both the upper and lower levels is primarily due to collisions with thermal electrons. The collisional deexcitation of the ith level is approximated by

$$D_i = \sum_j \int_E f(E)Q_{ij}^*(E)v(E)\,dE, \quad (7)$$

where $f(E)$ is a Maxwellian distribution with a mean energy of 0.1 eV and Q_{ij}^* is the deexcitation cross section from level i to level j.

The small signal gains are calculated as[16]

$$\gamma_0 = (\lambda^2/8\pi)A_{up}g(\nu)[N_u - (g_u/g_p)\ N_p], \quad (8)$$

where A_{up} is the Einstein's A coefficient for the transition between levels u and p, $g(\nu)$ is the Doppler broadened lineshape function, and λ is the wavelength.

The laser output power, for an inhomogeneously broadened transition is calculated as

$$P_0 = \frac{8\pi hc\,A}{\lambda^3 g(\nu)}\left[\left(\frac{\gamma_0 d}{L_i + T}\right)^2 - 1\right]T; \quad \gamma_0 > 0, \quad (9)$$

where T is the transmissivity of one mirror (the other is assumed 100% reflective) and, L_i represents the internal losses. The plasma length is d and A is the cross-sectional area of the active medium. We have assumed the total plasma volume is coupled to the resonator in the case of the transverse laser and have optimized the output mirror transmissivity for each set of gains.

The resonator configuration used by Hara *et al.* couples only a small fraction of the plasma volume to the TEM_{00} mode. We have calculated output power of the TEM_{00} mode as well as the approximate output power if higher-order modes are considered. In the latter case we have considered only modes of the form TEM_{nn}, including modes up to TEM_{77}. The TEM_{77} mode was the highest-order mode that was found to be able to oscillate under the excitation condi-

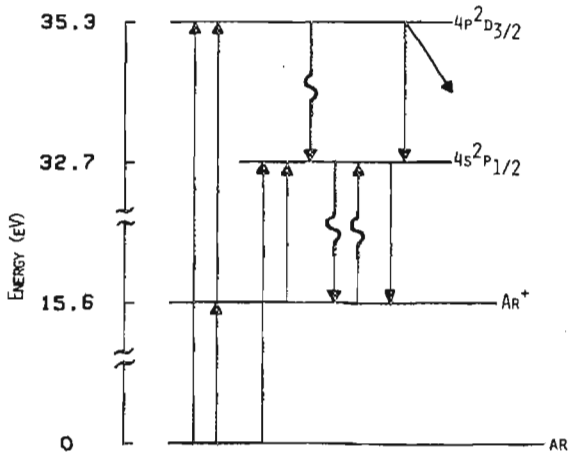

FIG. 4. Partial energy level diagram of Ar I and Ar II. These levels were used to calculate laser level populations. Straight lines indicate changes in state due to electron collision. Curved lines represent radiative transitions.

tions considered. We have numerically calculated the diffraction losses introduced by the 5-mm-diam cathode in the *e*-beam generation section of the laser for each of the modes. The diffraction losses have been incorporated into the output power equation. The power provided by each mode is calculated using the assumption that the TEM_{00} mode would dominate and the volume of the active region available for each successive mode is reduced by that of the lower-order modes thereby approximating mode competition in the active medium. We have assumed a mirror transmissivity of 3%, a cavity spacing of 3 m, and mirror curvatures of 3 m to match the cavity of Hara *et al.*

To include the effects of collisional heating of the gas in the laser medium the heat equation,

$$\nabla \cdot \lambda_a \nabla T_g = H, \tag{10}$$

was solved, for the gas temperature T_g using finite difference techniques for both the transverse and longitudinal devices discussed above. Here λ_a is the thermal conductivity of the gas and H represents gas heating terms due to elastic collisions of electrons and ions with neutral gas atoms. For the transverse device we have considered collisions of electrons with netural gas atoms in the negative glow region of the discharge and with ions in the sheath around the negatively biased reflector plate. We have assumed the device is contained in a water cooled vacuum envelope of 2 cm in width and that the cathode is ohmically heated to 1100 K. The reflector plate is considered to be heated by radiation from the cathode. In the longitudinal device, where the plasma tube diameter is much larger than the electron beam diameter,[5] we have assumed a wall temperature of 300 K.

The atom, ion, and electron temperatures are considered to be equal in the active region of the discharge. This assumption is reasonable in the electron-beam-created plasma due to the fact that there is essentially no electric field in the region, which is primarily a negative glow. Thus the electron temperature is low and approximately equal to the atomic and ionic temperatures. This phenomenon was observed in other discharges which are electron beam sustained.[11–13] Figure 5 illustrates the predicted averaged gas temperatures given by the heating model as a function of the input power conditions for the transverse device. Note that the scatter of the data shown in Fig. 5 is due to the fact that the device power is a function of both the beam accelerating voltage and the beam current density and as such two powers of the same value may actually represent two different operating regimes.

IV. RESULTS

In this section we discuss predicted gain, power, and efficiency of the electron-beam-pumped lasers discussed above, as functions of the electron beam energy, current, and gas pressure. We also include results which illustrate the relative importance of the mechanisms by which the laser levels are excited and deexcited. Model predictions for the transverse device are discussed first. Results for the longitudinally excited device are then compared with the experimental result obtained by Hara *et al.*

The major channel by which the electron beam energy is

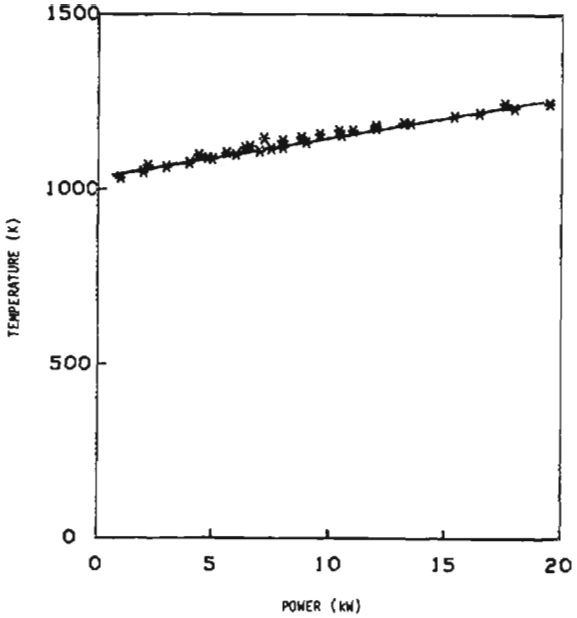

FIG. 5. Gas temperature as a function of input power. The fit parameter for the straight line are slope = 0.0184 K/W and intercept = 1020 K.

deposited in the discharge is through the ionization of ground-state argon atoms. This is shown in Fig. 6 which is a plot of the relative amount of energy deposited into the plasma through the various collision mechanisms as a function of the grid-to-cathode voltage (i.e., beam energy) at a current of 70 A (15.6 A/cm^2). The second most important mechanism is the excitation of ground-state atoms. Ionization of ground-state atoms accounts for 50%–70% of the electron beam energy deposited in the plasma with excitation collisions accounting for most of the balance. Other processes such as momentum transfer and ionization of the metastable state utilize less than 2% of the discharge energy. Because the cross sections for excitation of the upper laser levels are so much smaller than the cross sections for ioniza-

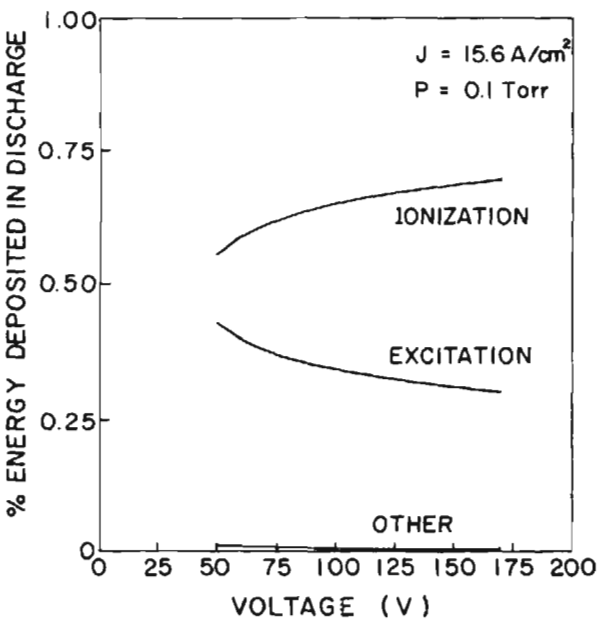

FIG. 6. Relative amount of electron beam energy deposited in the various collision channels.

tion and excitation of the neutral states (~ 100 times) the amount of beam energy deposited in excitation of the upper levels is quite small. As in the case of conventional argon ion lasers, this is one of the limiting factors in the efficiency of the electron-beam-pumped argon ion laser.

Figure 7 illustrates the dependence of the ground-state ion density on the electron beam current density with the grid-to-cathode voltage as a parameter. In the electron-beam-sustained discharge modeled here the dominant ionization mechanism is single-step ionization of ground-state atoms. Ionization of the neutral metastable state accounts for between 5% and 7% of the total ionization rate.

Hammer and Wen[6] used a low-energy electron-beam-pumped argon ion laser device to measure the direct electron impact excitation cross sections of several of the upper laser levels of the blue-green argon ion laser transitions. These cross sections have also been measured by Latimer and St. John[3] and Bennett.[17] We have used St. John's cross sections for all of the results discussed here except for one case in which the cross sections of St. John were normalized to the peak values obtained by Hammer for the sake of comparison. Hammer and Wen note the possibility of a factor of 2 error in their measurements. While Latimer and St. John give no error estimate, their measurements were made at much lower pressures thereby minimizing the effect of multiple collision processes as well as insuring the monoenergetic nature of the electron beam.

Hammer and Wen[3] measured the small signal gain coefficient the 4765-Å transition to be 0.002 cm^{-1} at a current density of 1.66 A/cm^2 and a voltage of 110 V. These measurements were conducted at a pressure of 0.1 Torr.[8] Running our model under these conditions yields a gain coefficient of 0.0015 cm^{-1} using St. John's cross sections and 0.0019 cm^{-1} using Hammer's cross sections. These results indicate a reasonable agreement between results provided by the model and the available experimental results.

Our simulations indicate that both direct excitation and two-step excitation of the lower upper levels play an important role in determining the upper laser level population in the electron-beam-excited laser. This can be seen in Fig. 8 which is a set of plots of the ratio of the two-step excitation rate, R_{mu} to the total excitation rate, on a per line basis, as a function of gas filling pressure for four different discharge conditions. Figures 8(a) and 8(b) were generated using a current density of 6.7 A/cm^2 corresonding to a total current of 30 A and grid to cathode voltages of 50 and 110 V, respectively. Figures 8(c) and 8(d) are plots for the same voltages as in 8(a) and 8(b) but a beam current density of 15.6 A/cm^2 which corresponds to a total device current of 70 A. Note that in all the plots the importance of the two-step mechanism decreases as the filling pressure is increased. This behavior of the electron–beam-pumped laser is in contrast to that of the conventional argon ion laser where an increase in pressure lowers the electron temperature and significantly decreases the single-step pumping rate. In the electron-beam-sustained discharge the electron energy distribution is less sensitive to changes in pressure than the positive column discharge in terms of the region of overlap with the collision excitation cross sections. The two-step dominance at low pressure is a result of the ion density being fairly constant with pressure while the ground-state density varies linearly with pressure. The following conclusions can be drawn from this group of plots: The 4765-Å transition is dominant-

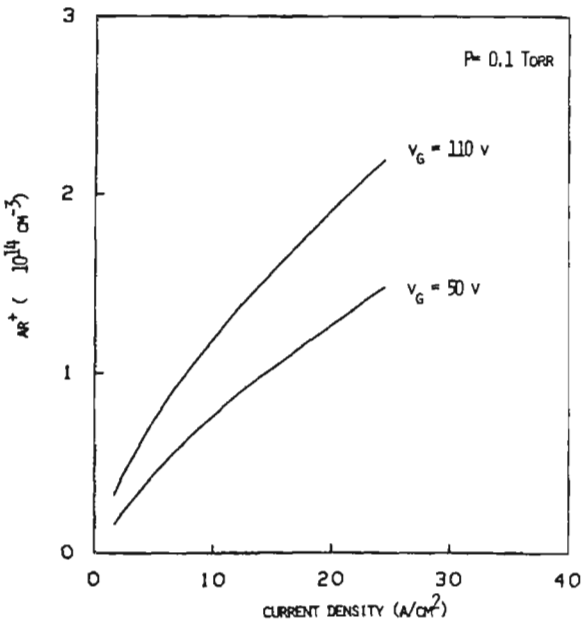

FIG. 7. Ground-state ion density as a function of electron beam current density for grid-to-cathode voltages of 50 and 110 V.

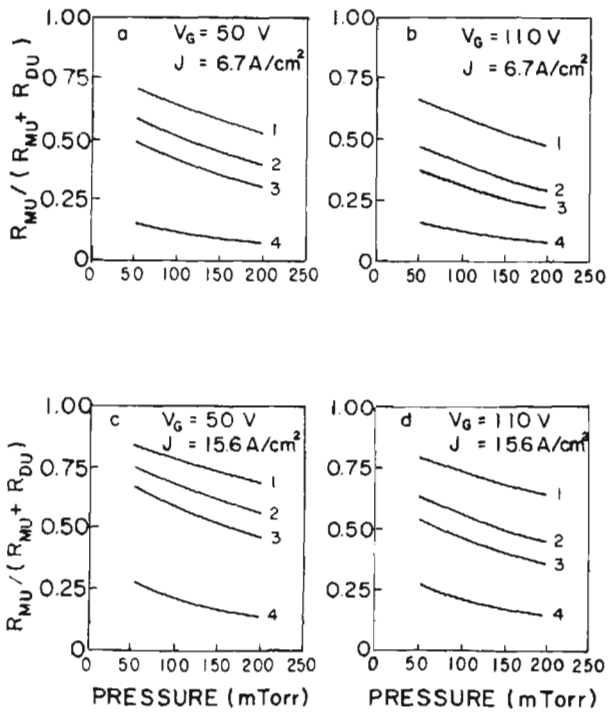

FIG. 8. Ratio of the two-step excitation rate to the total excitation rate of the upper laser levels as a function of the gas filling (a) $V_g = 50$ V, $J_m = 6.7$ A/cm^2, (b) $V_g = 110$ V, $J_m = 6.7$ A/cm^2, (c) $V_g = 50$ V, $J_m = 15.6$ A/cm^2, (d) $V_g = 110$ V, $J_m = 15.6$ A/cm^2. The numbers next to the curves on the graphs correspond to the following transitions: (1) 4880 Å, (2) 4965 Å, (3) 4658 Å, (4) 4765 Å.

ly pumped by single-step excitation for all the discharge conditions considered in this work while the 4880-Å transition is primarily driven by the two-step excitation mechanism. The remaining transitions are pumped by both mechanisms depending on the discharge conditions. The two-step mechanism is dominant at low pressures, low voltages, and high current densities.

Figures 9(a) and 9(b) are plots of the small signal gain coefficient, for the four transitions modeled, as a function of the grid to cathode voltage (i.e., beam energy) at current densities of 6.7 and 15.6 A/cm^2, respectively. In Figure 9(a) the gain of the 4880-Å transition drops off rapidly compared to the other lines. This is due to a combination of effects. The first factor is that the 4880-Å line is pumped primarily by two-step excitation and the cross section for this process drops off rapidly with increasing electron energy. As a result, as the beam energy is increased the total excitation rate saturates faster than the single-step excitation rates for the other laser lines. This can be seen in Fig. 10 which is a plot of the single-step and two-step excitation rates versus voltage for the 4765- and 4880-Å transitions. Coupling this factor with the fact that at higher ion densities trapping of the resonant radiation from the lower laser level preferentially reduces the gain of the 4880-Å transition, explains the more rapid decrease in gain of the 4880-Å line relative to the other transitions. Because the 4658- and 4880-Å transitions share the same laser lower level the effect of radiation trapping is also seen on the 4658-Å transition which shows a more rapid saturation with voltage than the 4765- and 4965-Å transitions. All of the transitions show saturation at high voltages due to increasing collisional deexcitation of the laser upper levels. Higher accelerating voltages correspond to a higher beam power density deposition and consequently a higher electron density. In Fig. 9(b) the same trends are observed. Again, all the transitions suffer from the effects of collisional deexcitation at the higher voltages.

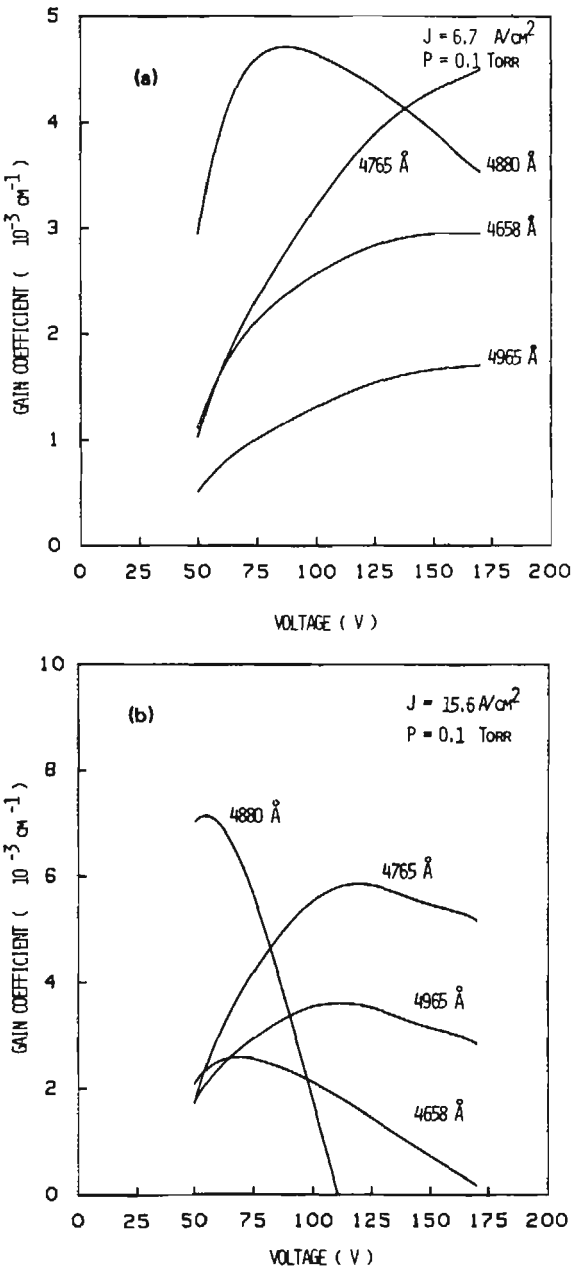

FIG. 9. Small-signal gain of the 4765-, 4880-, 4965-, and 4658-Å transitions as a function of the grid-to-cathode voltage. (a) $J_m = 6.7$ A/cm^2, (b) $J_m = 15.6$ A/cm^2. The argon pressure is 0.1 Torr.

The dependence of the optical gain coefficient of the four transitions on the electron beam current density is illustrated in Figs. 11(a) and 11(b) for gird to cathode voltages of 50 to 110 V, respectively. As seen in 11(a) the 4880-Å transition is dominant at low voltages for most of the current density range considered. This is because of the better match between the electron beam energy with the peak of the excitation cross section of the 4880-Å upper laser level. The cross section for excitation of the other levels peak at a higher energy. In 11(a) the effect of trapping of radiation from the $4s^2P_{3/2}$ level begins to be significant at current densities greater than 20 A/cm^2. From Fig. 7 this corresponds to an ion density of approximately 8×10^{13} cm^{-3}. The effect of radiation trapping on the $4s^2P_{1/2}$ laser lower level of the 4765- and 4965-Å transition begins to be significant at ion

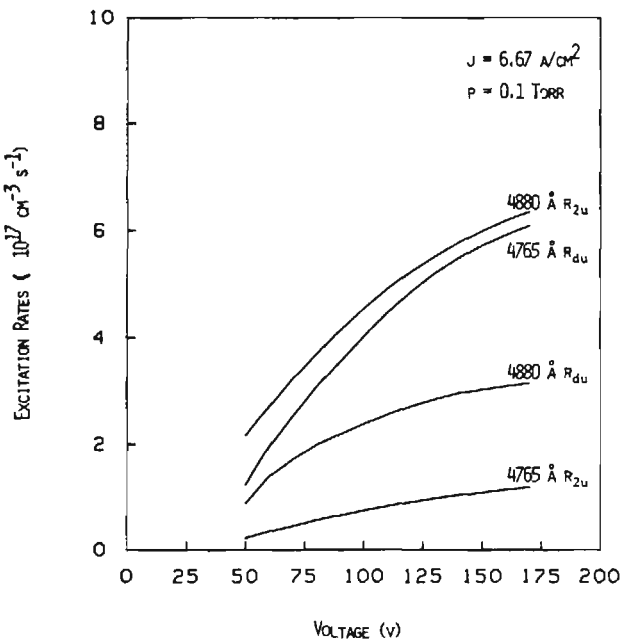

FIG. 10. Direct and two-step excitation rates for the upper laser levels of the 4765- and the 4880-Å transitions.

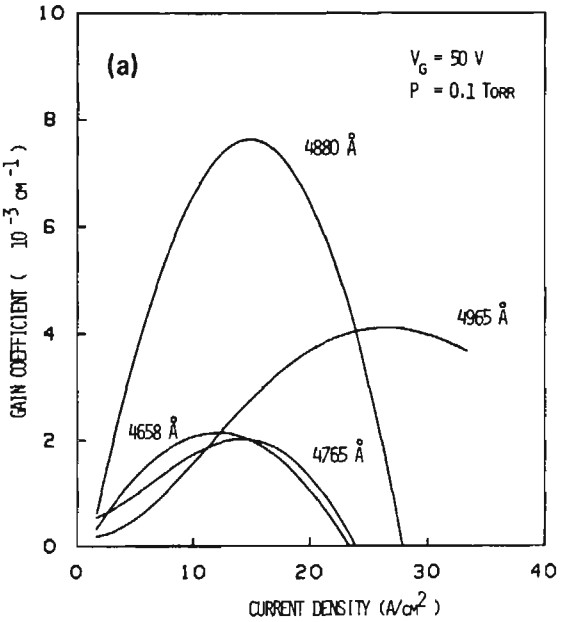

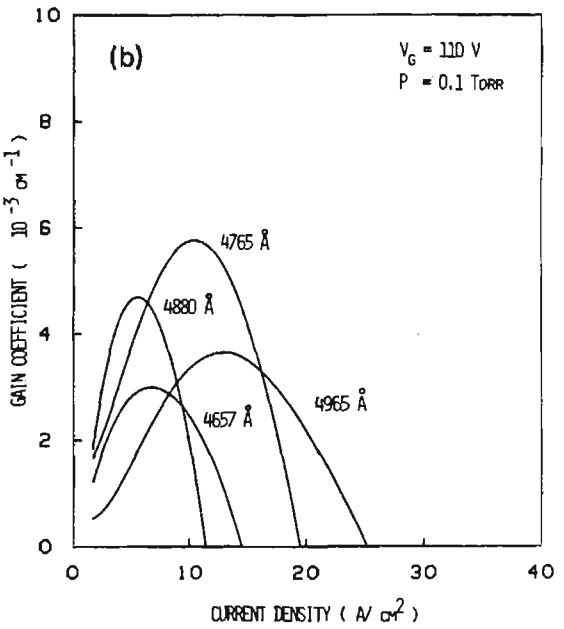

FIG. 11. Small-signal gain of the 4765-, 4880-, 4965-, and 4658-Å transitions as a function of the electron beam current density for two voltages (a) $V_g = 50$ V, (b) $V_g = 110$ V. The argon pressure is 0.1 Torr.

densities of approximately 1.5×10^{14} cm^{-3}. However, at current densities high enough to reach this plasma density the effect of collisional deexcitation has decreased the gain of these transitions beyond an operating range of any practical interest as can be seen in Fig. 11(b).

Figure 12 is a plot of the laser efficiency (ratio of laser output power to electron beam power), for the sum of the four transitions modeled, versus current density for grid-to-cathode voltages of 50 and 110 V. Assuming a totally reflective mirror at one end of the cavity and an output mirror whose reflectivity was optimized for an inhomogeneously broadened transition (i.e., $T = L_i$) the output powers corresponding to the peak coefficients of Fig. 12 are 820 and 950 mW, respectively. The peak efficiencies are predicted to be approximately 3.0×10^{-4}.

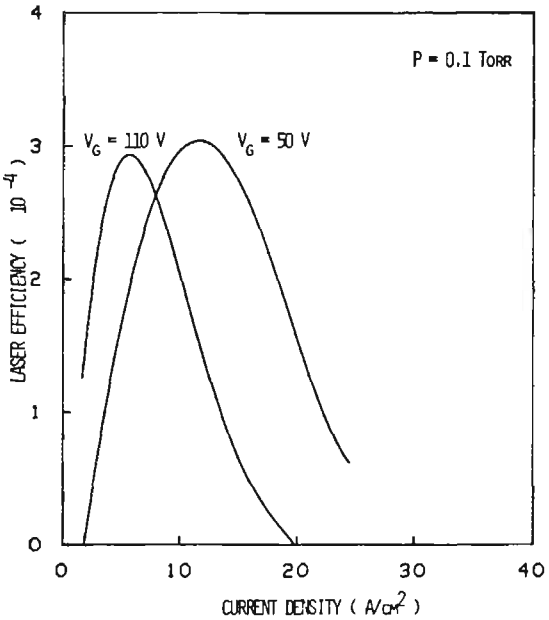

FIG. 12. Laser efficiency vs electron beam current density for grid-to-cathode voltages of 50 and 110 V. Only the 4765-, 4880-, 4965-, and 4658-Å transitions are considered in the efficiency calculations.

Hereafter we discuss the results of simulating the longitudinally excited electron beam argon ion laser developed by Hara *et al.*[5] Modeling of the longitudinal laser required the following assumptions: The electron beam plasma was assumed to be uniform over a diameter of 0.5 cm, which is the diameter of the smallest aperture in the beam generation section of the device. The longitudinal magnetic field contains the beam and minimizes beam spreading. We have assumed that the current reaching the active region of the discharge is equal to the total device current and that the rate of scattering of the beam electrons to the wall is small in the active region. The plasma length was estimated by calculating the reaching distance of the beam assuming that 20 eV is the average energy lost in an ionizing collision. At low pressures and high beam energies the reaching distance of the beam is longer than the length of the electromagnet, 45 cm, that surrounds the plasma tube. In these cases the active region is taken to be equal to the magnet length and the assumption of plasma uniformity is good. The approximation gets progressively worse as the accelerating voltage in the beam generation section of the device is reduced since the reaching distance of the beam gets shorter and as a result the plasma is probably not as uniform.

One of the most significant characteristics of the longitudinal laser is that Hara *et al.* have obtained oscillation on the 4880 Å, but none of the other well-known blue-green lines in the argon ion. Our simulations are consistent with the experimental results and show that, with the transmission losses of the resonator used by Hara *et al.*, only the 4880-Å transition has enough gain to oscillate. At the conditions that this device operates the strongest pumping mechanism is two step through the ion ground state. As shown previously the 4880-Å transition is pumped primarily by two-step excitation and has the largest cross section for two-step pumping of the four transitions modeled here. If the resona-

tor is optimized the other three transitions should indeed lase but relatively weakly in comparison to the 4880-Å line.

Figure 13 is a plot of the predicted output power of the longitudinal laser as a function of the gas pressure at a beam energy of 120 eV and a current of 9.0 A. Hara's results have been included for comparison. Hara *et al.* observed a peak power of 30 mW at a pressure of 53 mTorr. Our model predicts a peak multimode power of approximately 50 mW at a pressure of 85 mTorr. Notice that the experimental pressure was measured at either the inlet or outlet of the device and for the gas flowing scheme used in the experiment could easily be different than the pressure in the active region of the device. The rise of the output power, to the maximum, with increase in pressure is due to an increase in the proportion of electron beam energy deposited in the active medium. At low pressures much of the electron beam energy is not deposited in the active medium of the device but most of the electrons continue through the 45-cm active region without colliding and are forced to the walls of the discharge tube by the diverging magnetic field at the end of the solenoid. As the pressure is increased more of the electron beam power is deposited in the plasma. The decrease in power at high pressures is due to the onset of radiation trapping from the laser lower level which is a result of the increased ion density due to the increase in the amount of power deposited per unit volume.

The variation of the laser output power on the beam accelerating voltage, as predicted by the model, is shown in Fig. 14 at a current of 9.0 A and a pressure of 85 mTorr. The experimental results included in the figure are at a beam current of 9.0 A and a pressure of 53 mTorr. These pressure values represent the optimum operating pressure for the model and the actual laser, respectively. Good agreement is observed for the laser threshold at an electron beam accelerating voltage of approximately 60 V. The calculated peak value of the multimode power is within a factor of 2 of the experimentally obtained power and the TEM_{00} mode power is approximately 60% of the experimental result. The saturation of the output power with increasing voltage is due to trapping of the radiation from the laser lower level as the ion ground-state density increases with increasing input power. The effects of electron deexcitation of the upper laser levels also begin to be noticeable at the highest beam energies.

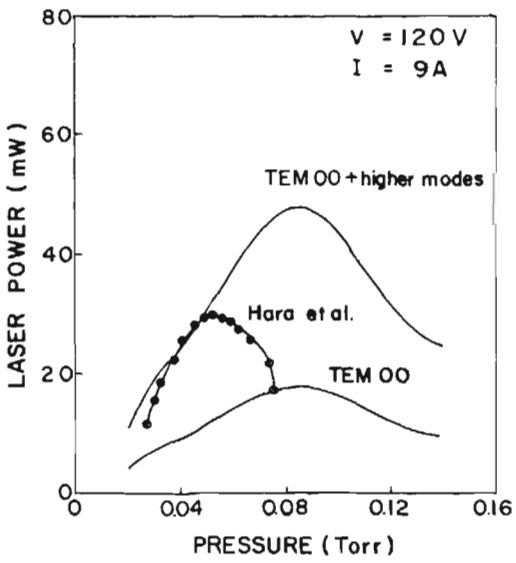

FIG. 13. Laser output power of the 4880-Å line as a function of the argon pressure in the laser tube.

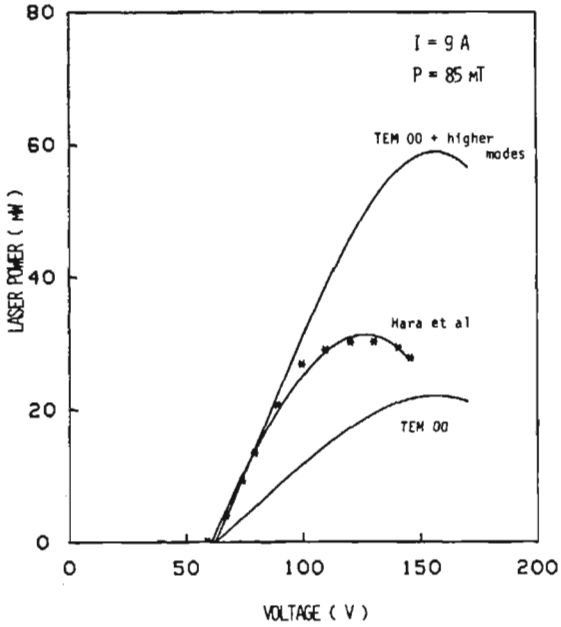

FIG. 14. Laser output power of the 4880-Å line as a function of the beam accelerating voltage. The experimental points of Hara *et al.* were measured at a pressure of 53 mTorr.

The dependence of laser output power on beam current is shown in Fig. 15 for an accelerating voltage of 120 V and a pressure of 85 mTorr. Again the results of Hara *et al.* are shown for sake of comparison and were taken at the optimum pressure. The slope of the multimode power curve is in good agreement with the slope of the experimental results, indicating that multimode oscillation is probably occurring.

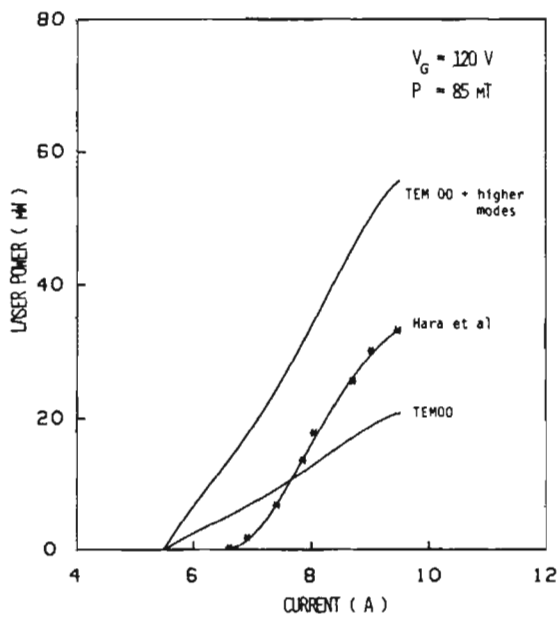

FIG. 15. Laser output power of the 4880-Å line as a function of the beam current. The experimental points of Hara *et al.* were measured at a pressure of 53 mTorr.

The peak efficiency obtained by Hara *et al.* approximately 3.0×10^{-5}. Model results indicate a peak efficiency of approximately 7.0×10^{-5} could be obtained if the transmissivity of the output coupler was optimized. If one considers the remaining blue-green lines in the argon ion, not included in our model, the efficiency of the device could be as high as 1.0×10^{-4}. Optimizing the geometry of the cavity to utilize more of the active plasma volume may add as much as a factor of 2 or 3 but this still is less efficient than the high-power conventional argon ion laser.

In summary, the electron-beam-pumped argon ion laser does not offer a significant improvement in efficiency over the more common high-power positive column lasers available commercially today. For example, a typical commercial argon ion laser,[18] has an operating efficiency of approximately 3.0×10^{-4} on the four transitions modeled here. This positive column laser has an overall efficiency of 4.0×10^{-4} if all the blue-green laser transitions in argon are considered. A similar overall efficiency would be expected in the electron beam laser. However, the electron-beam-pumped argon ion laser may be attracted as a source of blue-green radiation in applications requiring output powers on the order of 100 mW. Air-cooled positive column lasers of this type available on the market today generally have operating efficiencies which are significantly lower than that predicted by the model for the transverse electron-beam-pumped argon ion laser.

In reference to argon, the efficiency of the electron-beam-pumped laser is limited to low values for some of the same reasons that the positive column laser is an inefficient device. The amount of electron beam power that is spent in single-step electron impact excitation of the laser upper levels is a small fraction of the power deposited in the creation of ground-state ions, as expected from the relative size of the cross sections. A large fraction of these ions diffuse to the boundaries of the discharge before they can be excited to the upper laser levels by a second electron collision. The rate of loss of ground-state ions due to diffusion can be as large as two orders of magnitude than the two-step excitation of the upper laser levels. At increased electron beam current densities population of the upper laser levels through the ion ground state becomes increasingly important compared with diffusion; however, the laser output power and efficiency soon saturate due to trapping of the resonant radiation originating from the laser lower levels and by collisional electron deexcitation of the laser upper levels.

Electron beam excitation is advantageous when the energy stored in the ground-state ions is used to excite the laser upper levels. This is, for example, the case in charge transfer noble gas-metal vapor lasers.[19] In these devices the fact that most of the electron beam power is expended in the creation of noble gas ground-state ions is not a limitation, as in the case of the argon ion laser discussed in this work, but rather it is an advantage. The electron beam provides a large number of energetic electrons which can efficiently create ground-state noble gas ions at an optimum metal vapor density. These ions transfer their energy selectively to the laser upper level in the metal vapor specie by thermal charge transfer reactions. Due to the large cross section of these reactions, the relative loss of ground-state ions by diffusion is small. cw electron beam excitations of He-Zn and He-Hg lasers has shown an order of magnitude improvement in laser efficiency and output power over positive column and hollow cathode implementations.[19]

V. CONCLUSIONS

A computer model of cw electron-beam-pumped argon ion lasers has been developed which predicts small-signal gain coefficients which are in good agreement with gain measurements made by Hammer and Wen at low current densities and with laser output power measurements by Hara *et al.* The model predicts efficiencies of 3.0×10^{-4} can be obtained from the 4765-, 4880-, and 4658-, and 4965-Å, Ar II transitions with overall efficiencies expected to be approximately 4×10^{-4}. For a transverse device with an active medium 15 cm long and having a cross-sectional area of 0.3×0.3 cm^2 output powers of 1 W can be expected at input powers of 3.0 kW. Output powers of several hundreds of milliwatts could be obtained from a longitudinal device of the type build by Hara *et al.* if several steps toward optimization were completed. Thus the electron-beam-pumped argon ion laser would have an efficiency comparable to that of the multiwatt output power positive column devices available commercially. A possible practical use for the electron beam device may be in applications requiring low output powers and compact size in an air-cooled operating environment where the efficiencies of conventional devices is significantly lower.

The electron beam noble gas ion laser efficiency is limited by mechanisms similar to those which limit the positive column device. The major portion of the beam energy is used to create ground-state ions which diffuse to the walls of the discharge before they can be excited to the upper laser levels. Trapping of the radiation from the laser lower levels and collisional deexcitation of the laser upper levels also limit the output power and the efficiency of the electron-beam-excited argon ion laser at large (>15 A/cm^2) electron beam discharge current densities.

ACKNOWLEDGMENTS

This work supported by the National Science Foundation. The use of Class VI supercomputer time was made possible by the support from NSF grant no. QEWB8452009. One of the authors (J. Rocca) would like to acknowledge the support of an N. S. F. Presidential Young Investigators Award. The authors are grateful to Dr. B. E. Warner for the critical reading of this manuscript, to Dr. J. M. Hammer for his interest and cooperation with this effort, and to the careful help of J. Stockley and K. Lord in the preparation of the manuscript.

APPENDIX A: CROSS SECTIONS AND RATE CONSTANTS

Electron impact collision cross sections for levels in Ar I and Ar II were compiled in the process of modeling the cw electron-beam-pumped argon ion laser. Where possible, experimental data were used. Analytical expressions for the

TABLE I. Ionization cross-section parameters.

Parameters	A_0	A_1	A_2	A_3
Ground-state ionization	4.60	2.65×10^{-15}	1.20	250.00
Metastable ionization	2.00	3.25×10^{-15}	1.00	12.00

cross sections were obtained using curve fitting techniques. We discuss here the cross sections used in this model.

The ionization cross section was obtained by fitting the expression derived by Bretagne *et al.*[20] for the total ionization cross section, to the data of Rapp and Englander-Golden.[21] Bretagne includes an expression for the differential ionization cross section based on the same parameters used for the total ionization cross section. The same functional form was fit to the data of Vriens[22] to obtain the total ionization cross section of the metastable state.

The differential ionization cross sections have the functional form

$$Q_I(E_i,E_f) = A\left(\frac{A_0^2}{(E_i - E_f - I - E_0)^2 + A_0^2}\right), \quad \text{(A1)}$$

where I is the ionization threshold energy, E_i is the energy of the primary electron before the collision, and E_f is the final primary electron energy. Here

$$A = (A_1/E_i)\log_{10}(E_i/I) \quad \text{(A2)}$$

and

$$E_0 = A_2 - [A_3/(E_i + 2I)]. \quad \text{(A3)}$$

Table I contains the parameters A_0, A_1, A_2, and A_3 for both ionization cross sections.

The total ionization cross section is given by

$$Q_I(E) = \frac{A_1A_0}{E}\log_{10}\left(\frac{E}{I}\right) \times\left[\tan^{-1}\left(\frac{2A_0}{E - I - 2E_0}\right) - \tan^{-1}\left(\frac{A_0}{-E_0}\right)\right]. \quad \text{(A4)}$$

TABLE II. Excitation cross section parameters.

n	A_n	X_n
1	0.080	11.6
2	0.35	11.8
3	0.003	13.9
4	0.048	14.1
5	0.18	14.1
6	0.016	14.3
7	0.23	14.3
8	0.10	14.9
9	0.066	15.05
10	0.066	15.2
11	0.50	15.4
12	0.10	15.5
13	0.70	13.0

The cross sections required to calculate the excitation rates of the thirteen Ar I excited states considered in the model were taken from the work of Peterson and Allen.[23] They use a functional form introduced by Green and Barth where the parameters are depended on the level considered. The functional form of the cross section is

$$Q_n(E) = Q_0\frac{A_n}{X_n^2}\left(\frac{X_n}{E^\Omega}\right)\left(1 - \frac{X_n}{E}\right)^\nu, \quad \text{(A5)}$$

where $Q_0 = 6.513\times10^{-14}$. Here, $\Omega = 3/4$ and $\nu = 2$ except for the composite state, $n = 13$, where $\Omega = 1.5$ and $\nu = 1.0$. The parameters A_n and X_n are given in Table II.

An analytical expression for the elastic electron-argon momentum transfer cross section was obtained by fitting a least-squares polynomial to the data of Frost and Phelps.[24] The fit is given by

$$Q_m(E) = \begin{cases} 1.94\times10^{-17}(1 + 10.155E + 2.0104E^2 + 0.4332E^3 + 0.034556E^4 + 0.0008637E^5), & 0\leqslant E\leqslant 17\text{ eV} \\ 6.68\times10^{-16}e^{-8.68\times10^{-3}E} + 3.56\times10^{-15}e^{-9.196\times10^{-2}E}, & E\leqslant 17\leqslant E\leqslant 200. \end{cases} \quad \text{(A6)}$$

The reader is referred to the work of Ganas *et al.*[25] for the calculations regarding electron-electron collisions.

The Penning ionization coefficient was taken from the work of Ferreira.[26] The value of the coefficient used is $c = 1.0\times10^{-19}$ cm^3/s.

Cross sections for single-step excitations of the upper laser levels were taken from the experimental work of Latimer and St. John.[3] A cross section for the excitation of the 4765-Å line upper level from the ion ground state was taken from the theoretical work of Brandi and Koster.[27] Cross sections for excitation of the 4880-, 4658-, and 4965-Å upper levels from the ion ground state were obtained by fitting curves to the data of Imre *et al.*[28] Experimental data of Tan *et al.*[29] were used for the single-step excitation cross section of the lower laser levels.

Table III summarizes the necessary parameters for fitting the laser level excitation cross sections. Least squares polynomials were used for many of the fits. Where polynomials were used, the notation used in Table III is as follows:

$$Q(E) = \alpha\left(1 + \sum_{n=1}^{N} a_nE^n\right).$$

In cases where a cross section was fit using something other than a polynomial the expression is included in the table and a normalization coefficient is also given and will have a general form of

$$Q(E) = \alpha G(E).$$

Collisional deexcitation of the upper and lower laser levels was calculated using the theoretical cross section derived by Drawin[30] and the principle of detailed balance. The elec-

TABLE III. Laser level excitation cross-section parameters.

Cross section	α	Fit or coefficient	Valid energy region
Direct excitation $4p^2P_{3/2}$	$-1.36519298\times10^{-17}$	$a_1=-0.100554135$ $a_2=0.003427237$ $a_3=0.000050762$ $a_4=0.000000272$	$38<E<190$ eV
Direct excitation $4p^2P_{1/2}$	-6.5678447×10^{-18}	$a_1=-0.059778582$ $a_2=0.001324465$ $a_3=-0.000015080$ $a_4=9.327906\times10^{-8}$ $a_5=-2.973305\times10^{-10}$ $a_6=3.823227\times10^{-13}$	$35<E<190$ eV
Direct excitation $4p^2D_{5/2}$	-1.2663595×10^{-17}	$a_1=-0.060629884$ $a_2=0.001360111$ $a_3=-1.526648\times10^{-5}$ $a_4=9.046230\times10^{-8}$ $a_5=-2.597611\times10^{-10}$ $a_6=2.172645\times10^{-13}$ $a_7=2.589312\times10^{-16}$	$35<E<190$ eV
Direct excitation $4p^2D_{3/2}$	-8.905257×10^{-18}	$a_1=-0.060617056$ $a_2=0.001387184$ $a_3=-0.00001691$ $a_4=1.022036\times10^{-7}$ $a_5=-3.318196\times10^{-10}$ $a_6=4.343022\times10^{-13}$	$35<E<190$ eV
Multistep[a] excitation $4p^2P_{3/2}$	-1.365192×10^{-17}	$a_1=-0.10054135$ $a_2=0.003427237$ $a_3=-0.000050762$ $a_4=2.716804\times10^{-7}$	$19.85<E<68$ eV
	7.166×10^{-17}	$\log(E)/E$	$68<E<190$ eV
Multistep excitation $4p^2P_{1/2}$	-1.026839×10^{-17}	$a_1=-0.060389769$	$19<E<20$ eV
	-3.388726×10^{-15}	$a_1=-0.161724377$ $a_2=0.009740976$ $a_3=-0.00025908$ $a_4=2.567305\times10^{-6}$	$20<E<190$ eV
Multistep excitation $4p^2D_{5/2}$	-1.5470663×10^{-17}	$a_1=-0.0578986$	$17<E<20$ eV
	-8.778317×10^{-15}	$a_1=-0.1598698152$ $a_2=0.09493442$ $a_3=-0.000249204$ $a_4=-2.436947\times10^{-6}$	$20<E<28$ eV
	2.476×10^{-16}	$\log(E)/E$	$28<E<190$ eV
Multistep excitation $4p^2D_{3/2}$	$-1.54706635\times10^{-17}$	$a_1=-0.0578960$	$18<E<20$ eV
	-3.13687×10^{-15}	$a_1=-0.164045689$ $a_2=-0.010033760$ $a_3=0.000271462$ $a_4=-2.740700\times10^{-6}$	$20<E<28$ eV
	8.002443×10^{-17}	$\log(E)/E$	$28<E<190$ eV
Direct excitation $4s^2P_{1/2}$	-1.394657×10^{-17}	$a_1=-0.059926701$ $a_2=0.001398266$ $a_3=-1.670546\times10^{-5}$ $a_4=1.083549\times10^{-7}$ $a_5=-3.622886\times10^{-10}$ $a_6=4.888207\times10^{-13}$	$33<E<190$ eV

TABLE III. Continued.

Cross section	α	Fit or coefficient	Valid energy region
Direct excitation $4s^2P_{3/2}$	-2.538277×10^{-17}	$a_1 = -0.032926759$ $a_2 = 0.000768278$ $a_3 = -9.178826\times10^{-6}$ $a_4 = 5.953570\times10^{-8}$ $a_5 = -1.990597\times10^{-10}$ $a_6 = 2.685828\times10^{-13}$	$33<E<190$ eV

[a] Note that multistep excitation is excitation of the level from the ion ground state.

tron impact cross section for a transition from level i to level j is given by

$$Q_{ij}(E) = 4\pi a_0^2 (E_H/E_j - E_i)^2 f_{ij} g(u_{ij}), \quad \text{(A7)}$$

where a_0 is the Bohr radius, E_H is the hydrogen ionization energy, f_{ij} is the f value of the transition. $g(u_{ij})$ is defined as

$$g(u_{ij}) = \begin{cases} 0.302, & 1 \leqslant u_{ij} \leqslant 3.85, \\ (u_{ij}^{-1}/u_{ij}^2)\ln(1.25u_{ij}), & U_{ij} \geqslant 3.85, \end{cases}$$

where u_{ij} is calculated as

$$u_{ij} = (E/E_j - E_i).$$

APPENDIX B: A NUMERICAL SOLUTION TO THE BOLTZMANN EQUATION FOR ELECTRONS IN AN ELECTRON-BEAM-SUSTAINED NEGATIVE GLOW ARGON PLASMA

The electron energy distribution in an electron-beam-created plasma is non-Maxwellian. We have numerically solved the Boltzmann equation for electrons to calculate the electron energy distribution.[31]

The electron-beam-created plasma is practically field free. Electrons reflected by the plate may travel through the drift region several times since, under the conditions considered here, the reaching distance of the beam electrons is several times longer than the grid-to-plate spacing. This means the plasma is spatially uniform. Consequently, the Boltzmann equation may be solved in energy space rather than in phase space. Under these assumptions, the steady-state Boltzmann equation in the electron-beam-created plasma can be represented as collection of terms which we have written as[10]

$$-S(E) = P(E) - L(E) + C(E). \quad \text{(B1)}$$

The terms in Eq. (B1) represent the production and loss of electrons into and out of the energy interval $\{E,E+dE\}$. By discretizing the energy space into K energy bins of width w we can solve the equation numerically. $S(E)$ represents the flow of beam electrons into the plasma per unit volume per unit time, i.e., it is the source term. Because there is no electric field in the drift region the highest energy electrons in the plasma will be electrons injected at the beam energy. An electron may collide with an electron, an atom, or an ion and thus impart some of its energy to the other particle in either an elastic or inelastic fashion. This causes a loss of an electron from the bin corresponding to the initial energy and a production of an electron at some lower energy bin. The terms $P(E)$ and $L(E)$ are, respectively, the production and loss of electrons into and out of the bin corresponding to energy E due to inelastic collisions. The term $C(E)$ accounts for the production and loss of electrons into and out of the energy bin E due to elastic collisions.

A second type of mechanism by which electrons might be lost from an energy interval is by flowing out of the active plasma volume. This type of loss term was considered. Low-energy electrons, produced as secondary electrons in ionizing collisions or beam electrons having undergone many collisions, have a randomized motion. Thus, the kinetic flow of low-energy electrons may be viewed as diffusive. At low energies the electron loss rate should approach the diffusion rate. Electrons having energies close to the beam energy have a very directional motion. A diffusion rate approach is unsatisfactory in describing the flow of these electrons out of the volume. The approach selected to estimate the flow of electrons out of the laser volume was to define a probability distribution function, parameterized by the electron energy, which defines the probability of an electron approaching the edges of the volume at some angle. For low energies, the distribution approaches a uniform distribution, i.e., totally random motion of the electrons. At high energies the distribution is such that almost no electrons flow out of the sides of the volume. Beam electrons are lost primarily to the grid.

Several tests were performed to test the sensitivity of the model to both the functional form of the parameterized distribution and the overall importance of the flow-out loss term. Results showed little or no sensitivity to a wide range of distribution functions. Overall the flow-out loss rate for energetic electrons has little effect on the model predictions.

After discretizing, the energy space into bins of width w the continuous terms are converted to the form

$$P(k) = P(E = kw), \quad \text{(B2)}$$

where k is an integer ranging from 1 to K. K is defined as $K = \text{integer}(eV_g/w)$ where V_g is the grid-to-cathode voltage.

The electron beam is assumed to be monoenergetic, having the energy corresponding to the grid to cathode potential. The source term can be derived using Kirchoff's current law and take the form

$$S(k) = J_m \tau \frac{[1 - \exp(-2d/\lambda)]}{[1 - \tau\exp(-2d/\lambda)]}\delta(K-k), \quad \text{(B3)}$$

where J_m is the measured current density, V_g is the grid potential, and is the grid-to-plate spacing, τ is the grid transmissivity, and $\delta(k)$ is the Kronecker delta function. The term involving the exponentials accounts for those electrons

which do not collide in the plasma but are collected by the grid after being reflected by the negatively biased plate. Here λ is the collision mean free path of the beam electrons.

The energy of the electron beam in the source term is spent primarily in collisions with other particles in the plasma. The terms $P(k)$ and $L(k)$ include both ionization and excitation collisions. Single-step ionization from the ground state of the atom and two-step ionization through metastable levels are considered. The production of electrons into bin k due to inelastic collisions is

$$P(k) = P_I(k) + P_x(k). \tag{B4}$$

The contribution due to ionization $P_I(k)$ is made of the flow of primary electrons $P_1(k)$ and secondary electrons $P_2(k)$ into bin k such that

$$P_I(k) = P_1(k) + P_2(k), \tag{B5}$$

where

$$P_1(k) = \sum_{j=k+I}^{K_m} \mathrm{Ar} Q_I(j,k) V(j) Ne(j) w + \sum_{j=k+I_m}^{K_m^*} \mathrm{Ar}^* Q_{Im}(j,k) V(j) Ne(j) w \tag{B6}$$

and

$$P_2(k) = \sum_{j=2k+I}^{K_m} P_1(j-k-I) + \sum_{j=2k+I_m}^{K_m^*} P_{1m}(j-k-I_m).$$

Here $Q_I(j,k)$ and $Q_{Im}(j,k)$ are, respectively, the differential ionization cross sections for the ground-state and meatastable argon atoms. Ar is the density of ground-state neutral atoms. Ar* is the atomic metastable density. $V(j)$ and $Ne(j)$ are the velocity and density of electrons in energy bin j. K_m is defined as the minimum of either K or $2k+I$, where I is the ground-state ionization energy, and K_m^* is the minimum of K or $2k+I_m$, where I_m is the metastable ionization energy.

The production of electrons into bin k due to excitation collisions is given by

$$P_x(k) = \sum_n \mathrm{Ar} Q_n(k+E_n) V(k+E_n) Ne(k+E_n) w, \tag{B7}$$

where $Q_n(k)$ is the excitation cross section of the nth excited state and E_n is the bin corresponding to the excitation threshold of the nth level. We have considered the excitation of 12 allowed excited states and a single lumped metastable state in the argon atom.

Similarly, the loss of electrons from the k th energy bin is

$$L(k) = L_I(k) + L_x(k), \tag{B8}$$

where the loss of electrons from bin k due to ionizing collisions is

$$L_I(k) = \mathrm{Ar} Q_I(k) V(k) Ne(k) w + \mathrm{Ar}^* Q_{Im}(k) V(k) Ne(k) w,$$

where $Q_I(k)$ is the total ground-state ionization cross section and $Q_{Im}(k)$ is the total metastable state ionization cross section. The loss of electrons from energy bin k due to excitation collisions is

$$L_x(k) = \sum_n \mathrm{Ar} Q_n(k) V(k) Ne(k) w. \tag{B9}$$

The term $C(E)$ in Eq. (B1) represents the flow (in energy space) due to elastic collisions of electrons with ground-state atoms and with other electrons and is reduced to

$$C(k) = P_c(k) - L_c(k), \tag{B10}$$

where $P_c(k)$ represents the flow of electrons into bin k and $L_c(k)$ the flow out of bin k.

By adopting a bin formalism the problem of solving for the electron energy distribution is reduced to an algebraic problem. Note that all of the loss terms for the k th energy bin depend linearly on $Ne(k)$, making it possible to write

$$P(k) + P_c(k) + S(k) = Ne(k) T(k), \tag{B11}$$

where

$$Ne(k) T(k) = L(k) + L_c(k). \tag{B12}$$

The production terms $P(k)$ and $P_c(k)$ depend on the density of electrons in energy bins greater than k. The source term $S(k)$ is completely known and corresponds to the flow of electrons into the plasma volume at the beam energy. Thus beginning with the bin corresponding to the beam energy we may solve for $Ne(k)$ using the recursion

$$Ne(K-k) = [P(K-k) + S(K-k)/T(K-k)]; \quad k = 0,1,2,\ldots K-1. \tag{B13}$$

Because the rate of ionization depends on the metastable density and this population density depends on the electron energy distribution an iterative approach is necessary to successfully calculate the electron energy distribution, the metastble density, and the ion density in a consistent manner. The approach used is as follows: Initially a metastable density and an ion density are assumed. The electron energy distribution is then calculated. The system of equations for the ion and metastable populations presented in the main body of the paper are solved. The electron energy distribution is then recalculated. This process is repeated until all populations have converged.

[1] W. B. Bridges, in *Methods of Experimental Physics*, Vol. 15, Part A, "Quantum Electronics" (Academic, New York, 1979).
[2] M. H. Dunn and J. N. Ross, Prog. Quantum Electron. **4**, 233 (1976).
[3] J. D. Latimer and R. M. St. John, Phys. Rev. A **1**, 1612 (1970).
[4] J. M. Hammer and C. P. Wen, Appl. Phys. Lett. **7**, 161 (1965).
[5] T. Hara, Y. Sadamoto, M. Hamagaki, T. Ohgo, and T. Dote, J. Jpn. Phys.**22**, Part 2, 379 (1983).
[6] J. M. Hammer and C. P. Wen, J. Chem. Phys. **46**, 1225 (1967).
[7] J. M. Hammer (personal correspondence).
[8] P. K. Tien, D. McNair, and H. L. Hodges, Phys. Rev. Lett. **12**, 30 (1964).
[9] L. R. Peterson, Phys. Rev. **187**, 105 (1969).
[10] B. Warner, Ph.D. dissertation, Colorado University (1979).
[11] Z. Yu, J. J. Rocca, and G. J. Collins, Phys. Lett. **96A**, 125 (1983).
[12] J. R. McNeil, Ph. D. Dissertation, Colorado State University (1979).
[13] K. B. Persson, J. Appl. Phys. **36**, 3086 (1965).
[14] W. L. Weise, M. W. Smith, and B. M. Glennon, NSRDS-NBS, Vol. 2.
[15] T. Holstein, Phys. Rev. **83**, 1159 (1951).
[16] J. T. Verdeyen, *Laser Electronics* (Prentice-Hall, Inc., Englewood Cliffs, NJ, 1981).
[17] W. R. Bennett, Jr., J. W. Kuntson, Jr., G. N. Mercer, and J. L. Detch,

Appl. Phys. Lett. **4**, 180 (1964).
[18]*CR3, Coherent Radiation Argon Ion Laser Manual* (Coherent Radiation Inc., San Jose, CA).
[19]J. J. Rocca, J. D. Meyer, and G. J. Collins, Appl. Phys. Lett. **43**, 37 (1983).
[20]J. Bretagne, G. Delouya, J. Godart, and V. Puech, J. Appl. Phys. **14**, 1225 (1981).
[21]D. Rapp and P. Englander-Golden, J. Chem. Phys. **43**, 1464 (1965).
[22]L. Vriens, Phys. Lett. **8**, 260 (1964).
[23]L. R. Peterson and J. E. Allen, Jr., J. Chem. Phys. **56**, 6068 (1972).
[24]L. S. Frost and A. V. Phelps, Phys. Rev. **136**, 1538 (1964).
[25]P. Ganas, S. Dutta, and A. Green, Phys. Rev. A **12**, 111 (1970).
[26]C. R. Ferreira, Ph.D. dissertation, University de Paris Sud, Orsay (1976), p. 141.
[27]H. S. Brandi and G. F. Koster, Phys. Rev. **A 8**, 1303 (1973).
[28]A. I. Imre, A. I. Dashehenko, I. P. Zapesochnyi, and V. A. Kelman, Zh. Eksp. Teor. Fiz. **15**, 712 (1972).
[29]K. H. Tan, F. G. Donaldson, and J. W. McConkley, Can. J. Phys. **52**, 786 (1974).
[30]H. W. Drawin, Z. Phys. **225**, 483 (1969).
[31]G. J. Fetzer, J. J. Rocca, and G. J. Collins, 37th Gaseous Electronics Conference, Boulder, CO (unpublished) (1984).